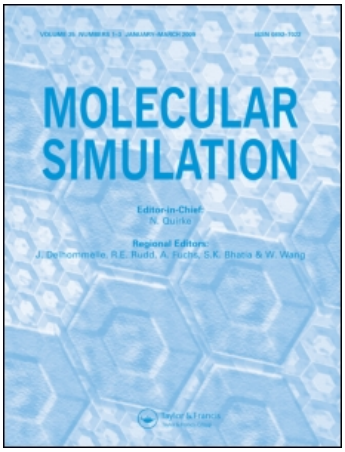

Molecular Simulation
Publication details, including instructions for authors and subscription information:
http://www.informaworld.com/smpp/title~content=t713644482

A study of synthesis gas conversion to methane and methanol over a Mo_6P_3 cluster using density functional theory

Sharif F. Zaman[a]; Kevin J. Smith[a]
[a] Department of Chemical and Biological Engineering, University of British Columbia, Vancouver, BC, Canada

To cite this Article Zaman, Sharif F. and Smith, Kevin J.(2008) 'A study of synthesis gas conversion to methane and methanol over a Mo_6P_3 cluster using density functional theory', Molecular Simulation, 34: 10, 1073 — 1084
To link to this Article: DOI: 10.1080/08927020802073040
URL: http://dx.doi.org/10.1080/08927020802073040

Molecular Simulation
Vol. 34, Nos. 10–15, September–December 2008, 1073–1084

Taylor & Francis
Taylor & Francis Group

A study of synthesis gas conversion to methane and methanol over a Mo_6P_3 cluster using density functional theory

Sharif F. Zaman and Kevin J. Smith*

Department of Chemical and Biological Engineering, University of British Columbia, Vancouver, BC, Canada

(Received 3 January 2008; final version received 12 March 2008)

Synthesis gas ($CO + H_2$) conversion to CH_4 and CH_3OH over a MoP catalyst has been examined using density functional theory and a Mo_6P_3 cluster model of the MoP surface. A model of synthesis gas conversion was developed by calculating adsorption energies of all possible arrangements of stable surface intermediates on Mo_6P_3. For CH_4 formation, the potential energy surface (PES) followed the route (H_{ad} addition at each step is assumed but not shown) $CO_{ad} \rightarrow CHO_{ad} \rightarrow CH_2O_{ad} \rightarrow CH_2OH_{ad} \rightarrow CH_{2.ad} + H_2O_{ad} \rightarrow CH_{3.ad} + H_2O_{ad} \rightarrow CH_4 + H_2O$ and CH_3OH followed $CO_{ad} \rightarrow CHO_{ad} \rightarrow CH_2O_{ad} \rightarrow CH_2OH_{ad} \rightarrow CH_3OH_{ad}$. The activation energy for the formation of CH_3OH from hydroxymethyl (100.9 kcal/mol) is higher than for the formation of methylene and water (40.3 kcal/mol), suggesting that CH_4 rather than CH_3OH will be produced from synthesis gas over MoP catalysts.

Keywords: synthesis gas; DFT; PES; methanol; methane; molybdenum phosphide

1. Introduction

The conversion of synthesis gas ($CO + H_2$) to alcohols and hydrocarbons using heterogeneous catalysts is well known. The production of CH_3OH using Cu/ZnO catalysts is practised commercially [1], as is the production of gasoline and diesel fuels via the Fischer–Tropsch synthesis using Fe or Co catalysts [2,3]. The selective conversion of synthesis gas to liquid fuels provides a route to renewable fuels that is almost CO_2 neutral, if the synthesis gas is produced from biomass. Our interest is in the selective conversion of synthesis gas to ethanol for use as a fuel or fuel additive. Several catalysts, based on metals such as Cu, Co, Pd and Fe, have been investigated for the higher alcohol synthesis [4] but few reports on the synthesis of ethanol from synthesis gas are available. Rhodium-based catalysts are able to produce oxygenates from synthesis gas [4,5]. The addition of appropriate promoters such as Mn enhance the rate of formation of these oxygenates, especially in the case of ethanol [5–10]. Mo-based catalysts also have high selectivity towards higher alcohols when Mo is doped with alkali metals [11]. Mo_2O_3 has also been used for the syngas conversion reaction [12], although, high ethanol selectivity was not achieved. The highest selectivity for ethanol has been reported on MoS_2 catalysts [13]. Interestingly, MoP supported on metal oxides (Al_2O_3, SiO_2), has been investigated as an alternative to MoS_2 catalysts for hydrodenitrogenation and hydrodesulfurisation reactions [14,15] and although there are no reports on the use of MoP for synthesis gas conversion to alcohols or hydrocarbons, previous researchers have suggested that metal phosphides may have good activity in other hydrogenation reactions, such as synthesis gas conversion to hydrocarbons and alcohols [16].

The use of computational chemistry in heterogeneous catalyst research and development has increased recently because of improved computational power and accuracy. Density functional theory (DFT) can be employed to calculate the formation energy of molecules and solids with high accuracy [17]. Information related to the surface reaction, such as heat of reaction, the reaction energy barrier and transition state (TS) structure, can also be determined. Computational chemistry can be used as a tool for catalyst design by calculating the catalyst's suitability for a particular reaction, without experimentation. Thus, a computational approach towards screening potential catalysts for a particular reaction is available and this principle has been reported in the literature [18]. Kubo et al. [17] used DFT to identify new catalyst formulations for methanol and Fischer–Tropsch synthesis based on the adsorption and formation energies of stable surface species on potential catalysts. Greeley and Mavrikakis [19] investigated the competitive methanol decomposition pathway on Pt(111) considering all combinations of stable surface species. Alcala et al. [20] used DFT to generate the reaction energy diagram

*Corresponding author. Email: kjs@interchange.ubc.ca

ISSN 0892-7022 print/ISSN 1029-0435 online

DOI: 10.1080/08927020802073040
http://www.informaworld.com

for ethanol decomposition on Pt(111). Similarly, a kinetic model of methanol decomposition on Pt(111) using DFT has been investigated by Gokhale et al. [21] and Kandoi et al. [22], who also reported the potential energy surface (PES) for this reaction.

As a first step in assessing MoP as a catalyst for synthesis gas conversion, especially to ethanol, we report herein on the reaction pathway for CH_3OH and CH_4 synthesis from CO and H_2 over an Mo_6P_3 cluster, determining the PES of the reactions. Due to limited experimental evidence of stable surface species over MoP, we investigated several likely stable surface species in each step of the reaction network and used the results of these calculations to determine the PES.

2. Methods

2.1 Calculation procedure

The DMol^3 module of Material Studio® (version 4.0) from Accelrys Inc. (San Diego, CA, USA) was used to complete the DFT calculations [23]. Accordingly, the electronic wave functions are expanded in numerical atomic basis sets defined on an atomic-centred spherical-polar mesh. The double-numerical plus *d*-function (DND) all electron basis set was used for all the calculations. The DND basis set includes one numerical function for each occupied atomic orbital and a second set of functions for valence atomic orbitals, plus a polarisation *d*-function on all atoms. The Becke exchange [24] plus Perdew–Wang approximation [25] non-local functional (GGA-PW91) was used in all the calculations. Each basis function was restricted to a cutoff radius of 4.5 Å, allowing for efficient calculations without loss of accuracy. The Kohn–Sham equations [26] were solved by a self-consistent field procedure. The techniques of direct inversion in an iterative subspace [27] with a size value of six and thermal smearing of 0.005 Ha [28] were applied to accelerate convergence. The optimisation convergence thresholds for energy change, maximum force and maximum displacement between the optimisation cycles were 0.00002 Ha, 0.004 Ha/Å and 0.005 Å, respectively. The *k*-point set of (1 × 1 × 1) was used for all calculations. The activation energy between two surface species was identified by complete linear synchronous transit and quadratic synchronous transit search methods [29,30], followed by TS confirmation through the nudge elastic band method [31]. Spin polarisation and symmetry were imposed in all the calculations.

2.2 Modelling approach

The Mo_6P_3 cluster model and the reactant and product species were created using the Material Studio Visualiser. The Cartesian positions of the atoms of the Mo_6P_3 cluster were fixed in a vacuum after performing geometry optimisation. The reactants and products were placed on the cluster in several different configurations, based on probable surface structures reported in the literature for CH_4 and CH_3OH synthesis. Geometric optimisation of each structure was then done with the atoms of the Mo_6P_3 cluster fixed and no constraints placed on the reactants and products. The adsorption energy was calculated by subtracting the energies of the gas phase species and the cluster from the energy of the adsorbed species according to the equation: $E_{ad} = E_{(adsorbate/cluster)} - (E_{adsorbate} + E_{cluster})$. With this definition, a negative E_{ad} corresponds to a stable surface species. The activation energy was calculated by using the TS search tool in DMol^3, applied to the reactant, a stable surface species plus an adsorbed H atom (H_{ad}) on the Mo_6P_3 cluster, and the product.

3. Results and discussion

3.1 An Mo_6P_3 cluster model of MoP

MoP has a hexagonal crystal structure, belonging to the $P_{\bar{6}m2}$ space group with lattice parameters $a = 3.22$ Å and $c = 3.19$ Å [16,33]. In the present study, an MoP crystal was built using the above information from which the (100) face was cleaved and a four atomlayer was taken as the cluster model, after geometric optimisation. Note that the cluster building unit resembles the (100) crystal face of MoP, as shown in Figure 1. The distances and angles between atoms for the cluster are tabulated in Table 1,

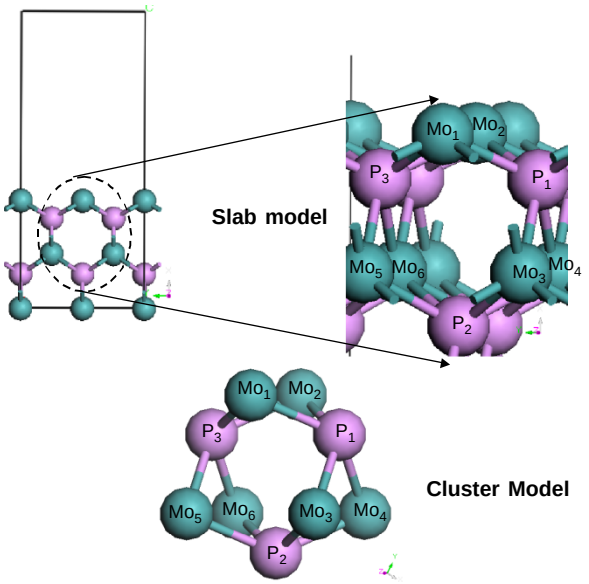

Figure 1. Comparison between MoP slab (100) face and the Mo_6P_3 cluster model of the present study.

Table 1. Comparison between Mo_6P_3 cluster and MoP (001) slab dimensions after geometric optimisation.

	Slab	Cluster*
Distances (Å)		
$Mo_{(1)}$-$Mo_{(2)}$	3.19	3.19
$Mo_{(1)}$-$P_{(1)}$	2.45	2.45
$Mo_{(3)}$-$P_{(1)}$	2.45	2.45
$Mo_{(3)}$-$P_{(2)}$	2.51	2.45
$Mo_{(1)}$-$P_{(2)}$	4.18	4.05
Angles (deg)		
$\theta_{Mo(1)\text{-}P(1)\text{-}Mo(3)}$	82.18	82.04
$\theta_{Mo(3)\text{-}P(2)\text{-}Mo(5)}$	79.74	82.18
$\theta_{Mo(1)\text{-}P(3)\text{-}Mo(2)}$	81.39	81.26
$\theta_{Mo(3)\text{-}P(2)\text{-}Mo(4)}$	78.85	81.26

*See Figure 1 for atom locations.

and these values compared favourably (within ±95%) to those of the MoP (100) slab. Mulliken population analysis showed a positive charge density (0.048*e*) on the Mo atoms and a negative charge density (−0.128*e*) on the P atoms of the cluster. Liu and Rodriguez [33] reported Mulliken charge densities of the MoP (001) crystal plane as 0.045*e* for Mo and −0.077*e* for P. Although, the electron charge on Mo is similar for the cluster and the (001) plane of MoP, the P atoms have higher electronegativity in the cluster compared to the MoP (001) plane. The difference is due to the metal rich stoichiometry of the Mo_6P_3 cluster.

3.2 *CO adsorption on the Mo_6P_3 cluster*

The adsorption energy of CO on the Mo_6P_3 cluster was calculated as −50.73 kcal, in very good agreement with values of −50.5 kcal [32] and −45.66 kcal [33] reported for CO adsorption on the (001) plane of MoP. The CO adsorption energies on Cu(111), Pd(111), Pt(111) and Ni(111), as reported in the literature, are summarised in Table 2. These data show that CO is adsorbed more strongly on MoP than any of these metals. For CO, the highest energy occupied molecular orbital (HOMO) is 5σ, a lone pair orbital, localised on the C atom. The lowest unoccupied molecular orbital (LUMO) is the 2π* orbital, a C—O π anti-bonding orbital also localised on the C atom. Hence, CO adsorbs on the Mo atom through the C atom. The LUMO energy of CO adsorbed on Mo_6P_3 is −75.18 kcal, the HOMO energy is −76.56 kcal and the Fermi level has energy −76.33 kcal. The HOMO energy is lower than the Fermi energy level and the LUMO is above the Fermi energy level, typical for surface chemisorbed species and hence, CO is strongly adsorbed on the Mo_6P_3 cluster. The density of states (DOS) of the Mo_6P_3 cluster compared to the DOS of the CO–Mo_6P_3 system, show that all the s (Figure 2(a)), p (Figure 2(b)) and d (Figure 2(c)) orbitals are altered. The d-orbital energy distribution, being the most affected, implies that the d-orbital of Mo is the main contributor to the adsorption process.

Table 2. Adsorption energy of CO and CH_3OH on transition metals.

Metal	CO adsorption energy (kcal)	CH_3OH adsorption energy (kcal)	References
Cu(111)	−16.14	−4.38	[19,37]
Pd(111)	−33.90	−6.46	[34]
Pt(111)	−41.97	−7.61	[22]
Ni(111)	−35.98	−0.46	[36]

3.3 *Determining the PES for CH_4 formation*

The search for the PES of CH_4 formation from H_2 + CO on the Mo_6P_3 cluster was accomplished by evaluating the adsorption energy of several possible surface intermediates and calculating the activation energy between two successive species. The reaction pathway for CH_4 (and CH_3OH) formation is depicted in Figure 3, where the surface reaction propagates by addition of H_{ad} to each stable adsorbed surface species. We have considered all combinations of H_{ad} attachment with the C and O atoms of CO. Bond angle, bond length and adsorption energies of adsorbed surface species and TS structures, heats of reaction and heats of adsorption are reported in Tables 3–5. The structure of the reactants, products and TSs are shown in Figures 4–6.

3.3.1 *Formyl (CHO) and hydroxymethylidyne (COH)*

The addition of H_{ad} to the C of CO_{ad} on Mo, yields CHO_{ad} species with the C and O attached to two nearby Mo atoms in a bridged structure (Figure 4(I)). The adsorption energy of this species was calculated as −94.32 kcal (Table 3). The addition of H_{ad} to the C atom of adsorbed CO species decreases the Mo—C bond strength, as indicated by an increase in bond length (1.99 Å) with respect to CO_{ad} on-top adsorption (1.97 Å). The Mo—O bond length is 2.10 Å. The hydroxymethylidyne (COH_{ad}) species is formed by addition of H_{ad} to the O atom of adsorbed CO_{ad} (Figure 4(II)). The C atom is bound to a Mo atom (on-top adsorption) and the Mo—C bond length decreases to 1.82 Å, indicating a more tightly bound surface species with higher adsorption energy (111.62 kcal) compared to CHO_{ad}. A higher adsorption energy for COH_{ad}, compared to CHO_{ad}, has also been observed on Cu(111) [19], Pd(111) [34] and Pt(111) [22] surfaces. The C—O bond length for CHO_{ad} is 1.31 vs. 1.34 Å for the COH_{ad} species, whereas, for CO_{ad}, it is 1.18 Å (Table 3). Increasing the CO bond length increases the C and O reactivity, as electrons are being accumulated on the atoms rather than being shared and the H_{ad} added to CO_{ad},

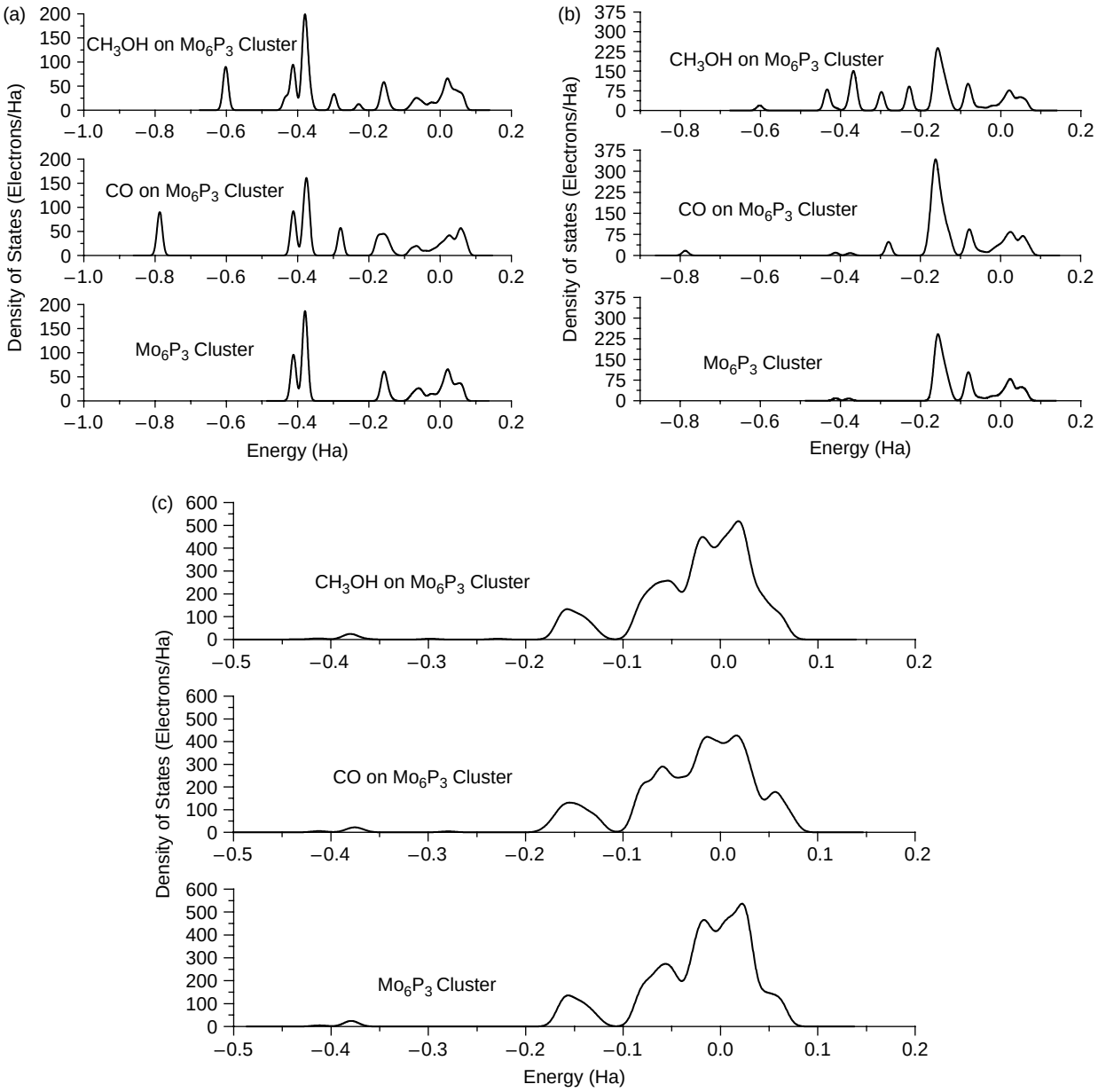

Figure 2. (a) DOS (s-orbital) of Mo_6P_3 cluster and CO and CH_3OH adsorbed on Mo_6P_3 cluster. (b) DOS (p-orbital) of Mo_6P_3 cluster and CO and CH_3OH adsorbed on Mo_6P_3 cluster. (c) DOS (d-orbital) of Mo_6P_3 cluster and CO and CH_3OH adsorbed on Mo_6P_3 cluster.

also weakens the C—O covalent bond strength. The activation energy associated with CHO_{ad} formation from $CO_{ad} + H_{ad}$ is 41.37 kcal/mol, whereas, for COH_{ad}, a value of 50 kcal/mol was obtained (Table 5). Formation of the CHO_{ad} is thermodynamically more favourable than the formation of COH_{ad}, and both reactions are endothermic, with a heat of formation of 10.13 kcal/mol for CHO_{ad} species and 49.50 kcal/mol for COH_{ad} species. Nunan et al. [35] reported CHO_{ad} as a precursor for alcohol production on copper based catalysts. The results presented herein suggest that CHO_{ad} is also the energetically favoured precursor for CH_4 and CH_3OH formation on the Mo_6P_3 cluster.

3.3.2 Formaldehyde (CH_2O) and hydroxymethylene (CHOH)

Addition of H_{ad} to the C atom of the formyl species forms CH_2O_{ad} (Figure 4(IV)), with an adsorption energy of -67.79 kcal. The Mo—C bond length is 2.22 Å and the Mo—O bond length is 1.96 Å. Compared to the CHO_{ad} species, the Mo—C bond length is increased, whereas, the

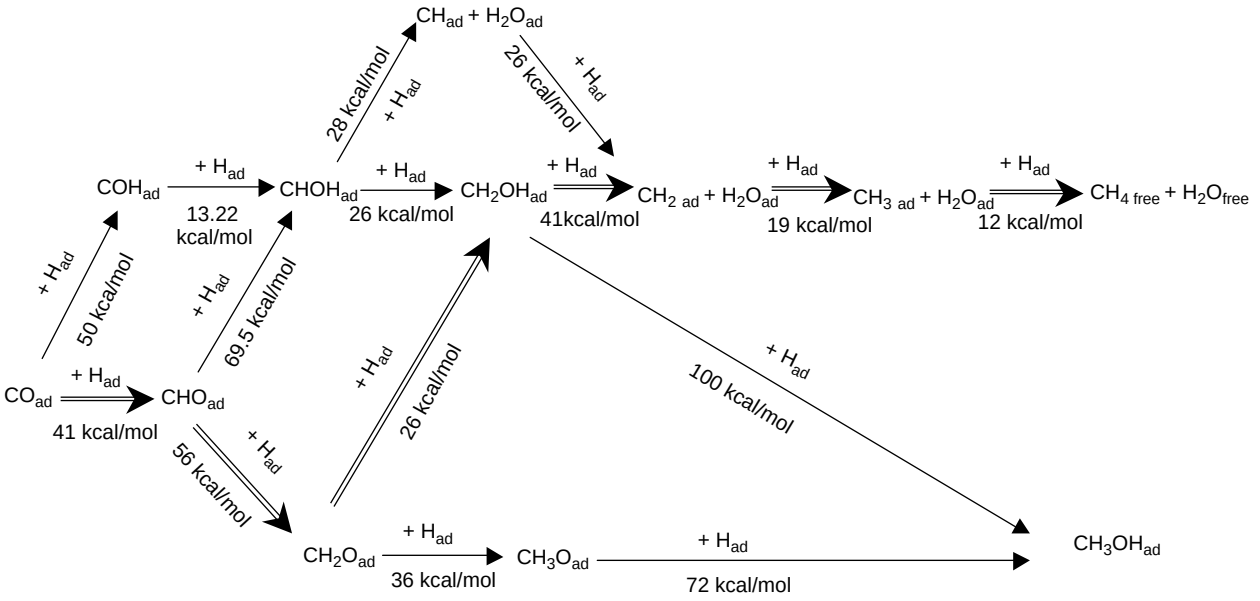

Figure 3. Reaction network and activation energies for syngas conversion to methanol and methane over the Mo_6P_3 cluster.

Mo—O bond length is decreased, CH_2O_{ad} is tightly bound through the Mo—O and electrons are withdrawn from the substrate by the O atom. The C—O bond length (1.41 Å) increases compared to CHO_{ad} (Table 3). The molecular orbital of the CH_2O_{ad} species weakens the C—O bond strength. The π electron interaction between CH_2 (π bonding and anti-bonding orbitals) and O (π type loan pair electron) gives rise to a new molecular orbital. Since, the energies of these interacting orbitals are similar, the new orbital is C—O anti-bonding and C—H bonding. If a H atom adds to the O atom of adsorbed CHO_{ad} species, $CHOH_{ad}$ is formed (Figure 4(V)) with an adsorption energy of -96.63 kcal. The Mo—C bond length (1.95 Å) decreases and the Mo—O bond length (2.33 Å) increases compared to the adsorbed CHO_{ad} species. The C—O bond length for CH_2O_{ad} species (1.41 Å) is higher than CHO_{ad}, but lower than $CHOH_{ad}$ (Table 3).

The activation energy for CH_2O_{ad} formation is 56.24 kcal/mol compared to 69.53 kcal/mol for $CHOH_{ad}$ (Table 5). Formation of CH_2O_{ad} is thermodynamically more favourable; formation of CH_2O_{ad} is exothermic ($\Delta E_r = -3.25$ kcal/mol) whereas, formation of $CHOH_{ad}$ is endothermic ($\Delta E_r = 2.59$ kcal/mol). $CHOH_{ad}$ can also be formed by the addition of H_{ad} to COH_{ad} (Figure 4(III)) with a lower activation energy (13.22 kcal/mol) and formation energy of 2.59 kcal/mol (Table 5) compared to H_{ad} addition to CHO_{ad}. This route is important for the decomposition of CH_4 and CH_3OH to CO and H_2.

Table 3. Properties of surface adsorbed species on Mo_6P_3 cluster from DFT calculations: angle to the surface, distance between atoms, total energy and adsorption energy of stable surface species relevant to methane and methanol formation from syngas.

Species	Figure	$\theta_{C-Mo-Mo}$ (deg)	$\theta_{O-Mo-Mo}$ (deg)	d_{C-Mo} (Å)	d_{O-Mo} (Å)	d_{C-O} (Å)	$E_{element}$ (au)	E_{ad} (kcal)
CO_{ad}	–	78.28	–	1.97	–	1.18	−113.345	−50.73
CHO_{ad}	4(Ic)	57.68	66.22	1.99	2.10	1.31	−113.857	−94.32
COH_{ad}	4(IIc)	77.27	–	1.82	–	1.34	−113.782	−111.62
$CHOH_{ad}$	4(IIIc)	68.15	63.22	1.95	2.33	1.44	−114.403	−96.63
CH_2O_{ad}	4(IVc)	59.70	70.43	2.22	1.96	1.41	−114.504	−67.79
CH_2OH_{ad}	4(VIc)	67.50	67.95	2.22	1.96	1.41	−115.052	−77.02
CH_3O_{ad}	6(XIVc)	–	119.32	–	1.92	1.41	−115.047	−109.08
CH_3OH_{ad}	6(XIIIc)	–	110.03	–	2.32	1.45	−115.711	−33.21
$CH_{ad}+H_2O_{ad}$	5(VIIIc)	97.67	78.86	1.82	2.29	3.02	−38.457	−173.42
$CH_{2.ad}+H_2O_{ad}$	5(IXc) and (Xc)	97.60	79.28	1.96	2.30	3.05	−39.130	−145.97
$CH_{3.ad}+H_2O_{ad}$	5(XIc)	123.65	85.80	2.16	2.36	4.26	−39.814	−66.42
$CH_4+H_2O_{free}$	5(XIIc)	Free	Free	2.65	2.39	–	−40.492	46.35

Energy of free $H_2O = -76.422778$ au. Adsorption energy of hydrogen atom $= -0.58213$ au. [au = atomic unit]

Table 4. Properties of surface adsorbed species on Mo_6P_3 cluster from DFT calculations: angle to the surface, distance between atoms, total energy and adsorption energy of stable surface species relevant to methane and methanol formation from syngas.

Species	Figure	$\theta_{C-Mo-Mo}$ (deg)	$\theta_{O-Mo-Mo}$ (deg)	d_{C-Mo} (Å)	d_{O-Mo} (Å)	d_{C-O} (Å)	$E_{element}$ (au)	E_{ad} (kcal)
$CO_{ad} + H_{ad}$	4(Ia)	78.23	–	1.98	–	1.18	−113.345	−62.03
$CO_{ad} + H_{ad}$	4(IIa)	78.89	–	1.99	–	1.18	−113.345	−61.11
$CHO_{ad} + H_{ad}$	4(IVa)	52.98	66.41	1.99	2.10	1.30	−113.857	−106.31
$CHO_{ad} + H_{ad}$	4(Va)	57.47	66.31	1.99	2.10	1.30	−113.857	−106.31
$COH_{ad} + H_{ad}$	4(IIIa)	78.40	–	1.82	–	1.33	−113.782	−123.61
$CHOH_{ad} + H_{ad}$	4(VIa)	67.89	63.57	1.97	2.23	1.44	−114.403	−117.84
$CHOH_{ad} + H_{ad}$	5(VIIIa)	68.53	63.26	1.94	2.29	1.47	−114.403	−85.09
$CH_2OH_{ad} + H_{ad}$	5(IXa)	69.17	66.46	2.20	2.28	1.49	−115.052	−54.88
$CH_2OH_{ad} + H_{ad}$	6(XIIIa)	67.70	67.03	2.21	2.23	1.48	−115.052	−86.94
$CH_2O_{ad} + H_{ad}$	4(VIIa)	58.21	71.71	2.23	1.96	1.41	−114.504	−81.86
$CH_3O_{ad} + H_{ad}$	6(XVa)	–	128.83	–	1.92	1.41	−115.047	−120.61
$CH_{ad} + H_2O_{ad} + H_{ad}$	5(Xa)	96.02	78.83	1.81	2.27	2.98	−38.457	−192.56
$CH_{2.ad} + H_2O_{ad} + H_{ad}$	5(XIa)	96.08	78.89	1.97	2.29	2.97	−39.130	−103.31
$CH_{3.ad} + H_2O_{free} + H_{ad}$	5(XIIa)	123.18	–	2.16	2.36	4.23	−39.814	−81.64

3.3.3 *Hydroxymethyl (CH_2OH)*

CH_2OH_{ad} species can evolve either by addition of H_{ad} to the C atom of $CHOH_{ad}$ species or by the addition of H_{ad} to the O atom of adsorbed CH_2O_{ad} (Figure 4(VI) and (VII)). The calculated adsorption energy of CH_2OH_{ad} on the Mo_6P_3 cluster was −77.02 kcal. The bond lengths are Mo—C 2.22 Å, Mo—O 1.96 Å and C—O 1.41 Å. These lengths are close to those calculated for the CH_2O_{ad} species, whereas, compared to $CHOH_{ad}$, the Mo—C bond length is increased and the Mo—O and the C—O bond-lengths are decreased. The activation and reaction energies for $CH_2O_{ad} + H_{ad} \rightarrow CH_2OH_{ad}$ are 59.12 and 34.56 kcal/mol, respectively, and for the $CHOH_{ad} + H_{ad} \rightarrow CH_2OH_{ad}$ they are 25.67 and 0.49 kcal/mol, respectively.

3.3.4 *C—O bond scission and the formation of CH_4*

Three intermediates are relevant for C—O bond scission: COH_{ad}, $CHOH_{ad}$ and CH_2OH_{ad}. Bond scission from COH_{ad} is described in a later section that discusses carbon formation on the catalyst surface. Adding H_{ad} to $CHOH_{ad}$ yields CH_{ad} (carbene) species and H_2O_{ad}, whereas, adding H_{ad} to CH_2OH_{ad} forms $CH_{2.ad}$ (methylene) and H_2O_{ad}.

Table 5. Properties of TS for reactions shown: structure, angle with the surface, distance between atoms, energy of reaction and activation energy for methane and methanol formation from syngas.

Reactions	$\theta_{C-Mo-Mo}$ (deg)	$\theta_{O-Mo-Mo}$ (deg)	d_{C-Mo} (Å)	d_{O-Mo} (Å)	d_{C-O} (Å)	ΔE_r (kcal/mol)	ΔE (kcal/mol)
Common (see Figure 4)							
$CO_{ad} + H_{ad} \rightarrow CHO_{ad}$	70.99	–	1.98	–	1.18	10.13	41.37
$CO_{ad} + H_{ad} \rightarrow COH_{ad}$	82.83	–	1.92	–	1.24	49.50	50.00
$CHO_{ad} + H_{ad} \rightarrow CHOH_{ad}$	65.08	62.87	1.98	2.32	1.32	32.95	69.53
$COH_{ad} + H_{ad} \rightarrow CHOH_{ad}$	40.40	–	2.07	–	1.36	2.59	13.22
$CHO_{ad} + H_{ad} \rightarrow CH_2O_{ad}$	56.09	67.76	2.01	2.11	1.30	−3.25	56.24
$CHOH_{ad} + H_{ad} \rightarrow CH_2OH_{ad}$	68.23	63.29	1.96	2.23	1.47	0.49	25.67
$CH_2O_{ad} + H_{ad} \rightarrow CH_2OH_{ad}$	70.21	62.48	2.22	2.15	1.45	34.56	59.12
Methane synthesis (see Figure 5)							
$CHOH_{ad} + H_{ad} \rightarrow CH_{ad} + H_2O_{ad}$	96.09	82.61	1.80	1.98	3.16	−5.87	42.16
$CH_{ad} + H_{ad} + H_2O_{ad} \rightarrow CH_{2.ad} + H_2O_{ad}$	93.83	79.96	1.83	2.23	2.94	−5.45	60.94
$CH_2OH_{ad} + H_{ad} \rightarrow CH_{2.ad} + H_2O_{ad}$	94.31	76.84	1.80	1.99	2.88	−6.19	27.88
$CH_{2.ad} + H_{ad} + H_2O_{ad} \rightarrow CH_{3.ad} + H_2O_{ad}$	110.36	82.63	1.97	2.35	3.62	−6.01	18.67
$CH_{3.ad} + H_{ad} + H_2O_{ad} \rightarrow CH_{4.ad} + H_2O_{ad}$	118.95	–	2.11	2.36	4.39	8.70	12.16
Methanol synthesis (see Figure 6)							
$CH_2O_{ad} + H_{ad} \rightarrow CH_3O_{ad}$	63.04	83.21	2.38	2.13	1.33	−6.22	71.13
$CH_3O_{ad} + H_{ad} \rightarrow CH_3OH_{ad}$	–	112.98	4.74	2.03	1.42	36.65	71.54
$CH_2OH_{ad} + H_{ad} \rightarrow CH_3OH_{ad}$	62.62	73.94	2.30	2.28	1.52	8.45	100.91

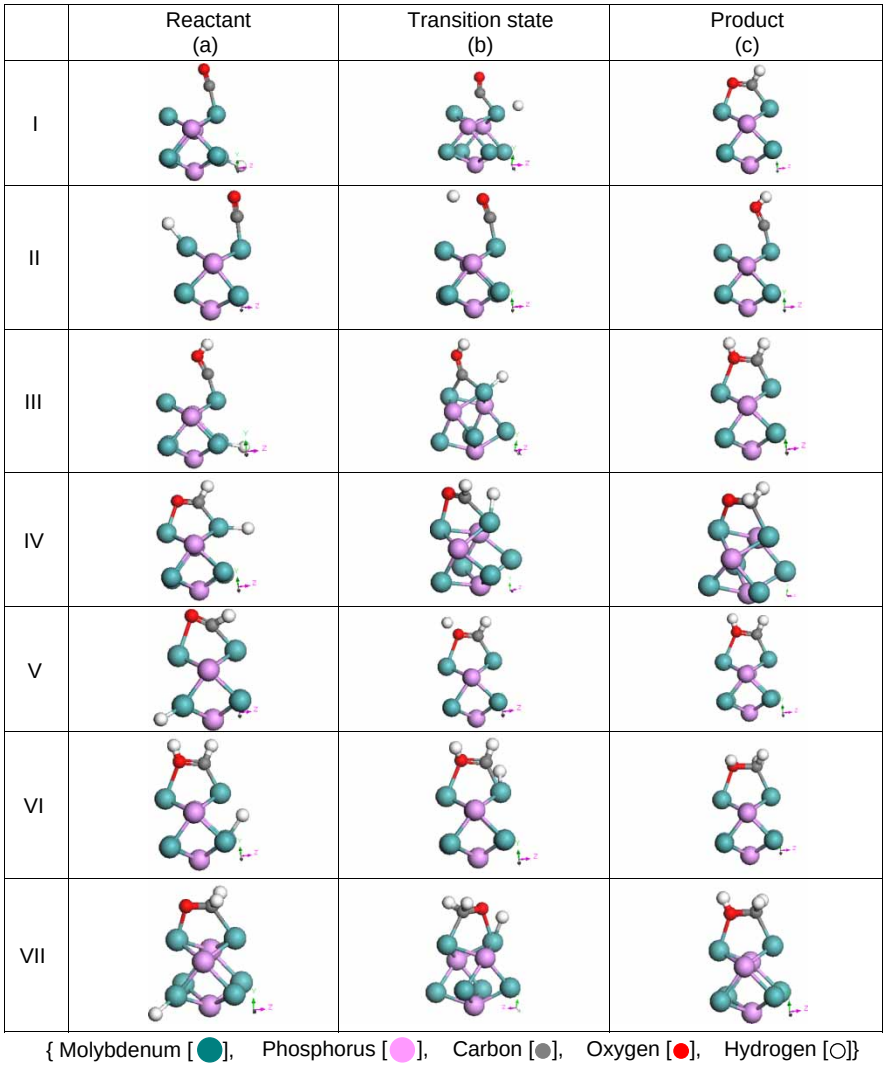

Figure 4. Methane and methanol formation reaction steps on Mo_6P_3 cluster.

These steps are shown in Figure 5(VIII) and (IX), respectively. The adsorption energies of $CH_{ad} + H_2O_{ad}$ and $CH_{2.ad} + H_2O_{ad}$ are -173.42 and -145.98 kcal, respectively. The Mo—C bond length is 1.82 Å for CH_{ad} species and 1.96 Å for $CH_{2.ad}$ species. CH_{ad} species are more strongly adsorbed on the surface than $CH_{2.ad}$ species. With two H atoms attached to the O atom, the octet condition for O, the most stable condition, is satisfied. The H_2O_{ad} molecule subsequently desorbs from the catalyst surface. The activation energy for C—O bond scission via the $CHOH_{ad}$ route is 42.16 kcal/mol, whereas, via the CH_2OH_{ad} route it is 27.88 kcal/mol (Table 5). Bond breakage results in heat generation with $CHOH_{ad} + H_{ad} \rightarrow CH_{ad} + H_2O_{ad}$ yielding $\Delta E_r = -5.87$ kcal/mol and $CH_2OH_{ad} + H_{ad} \rightarrow CH_{2.ad} + H_2O_{ad}$ yielding -6.19 kcal/mol.

Addition of H_{ad} to CH_{ad} species yields $CH_{2.ad}$ species (Figure 5(X)). The H_2O_{ad} molecule produced by the C—O bond scission is adsorbed on a Mo atom and the total adsorption energy of $CH_{2.ad} + H_2O_{ad}$ is -145.97 kcal with an adsorption energy of H_2O_{ad} on the cluster calculated as -32.52 kcal. Separate calculations for the CH_{ad}, $CH_{2.ad}$ and $CH_{3.ad}$ species on the cluster yielded adsorption energies of -116.23, -106.08 and -80.94 kcal, respectively. The total adsorption energy for $CH_{2.ad} + H_2O_{ad}$ is marginally lower than the sum of the energies of the separately adsorbed species in the system, likely due to interaction effects between the adsorbed species. The activation energy for this reaction step is 60.94 kcal/mol with an exothermic reaction energy $\Delta E_r = -5.45$ kcal/mol.

Addition of H_{ad} to $CH_{2.ad}$ yields adsorbed $CH_{3.ad}$ species. The Mo—C bond length associated with the $CH_{3.ad}$ intermediate increased to 2.16 Å and the adsorption energy decreased to -66.42 kcal compared to the adsorbed $CH_{2.ad}$ species. The activation energy for

	Reactant (a)	Transition state (b)	Product (c)
VIII	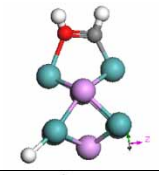	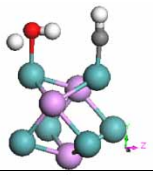	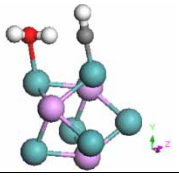
IX	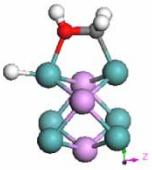	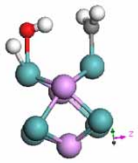	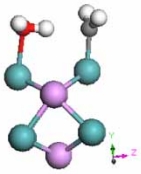
X	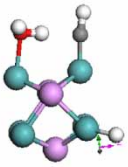	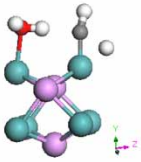	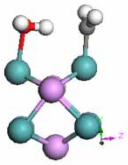
XI	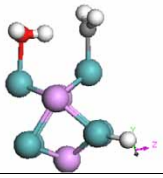	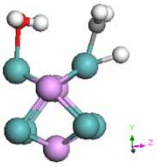	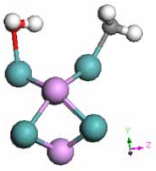
XII	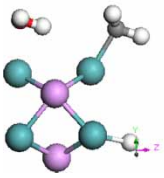	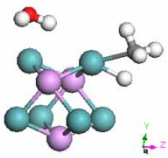	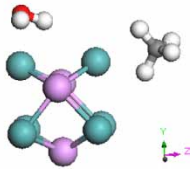

Figure 5. Methane formation reaction steps on Mo_6P_3 cluster.

	Reactant (a)	Transition state (b)	Product (c)
XIII	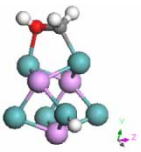	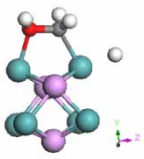	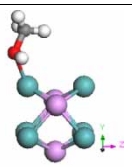
XIV	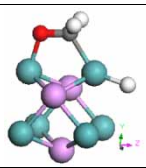	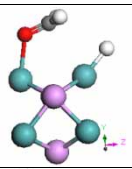	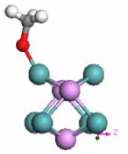
XV	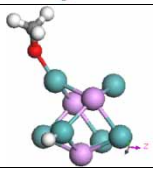	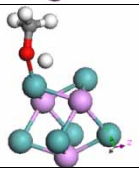	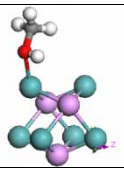

Figure 6. Methanol formation reaction steps on Mo_6P_3 cluster.

the process is 18.67 kcal/mol with an exothermic heat of reaction $\Delta E_r = -6.01$ kcal/mol. The reaction step is depicted in Figure 5(XI).

Adding another H_{ad} to the C atom of $CH_{3.ad}$ species forms CH_4. Both the CH_4 molecule and the H_2O_{ad} molecule are desorbed from the surface. CH_4 has a positive adsorption energy (46.35 kcal), indicating that CH_4 is not adsorbed on the surface at the simulation temperature (273 K). Consequently, once CH_4 is formed it will not engage in further reaction and will emerge as a product. The activation energy of this step is 12.16 kcal/mol. The reaction is endothermic and the reaction energy is 8.7 kcal/mol. Figure 5(XII) shows this reaction step.

3.3.5 *Carbon formation on the surface*

Addition of H_{ad} to the O atom of CO_{ad}, rather than to the C atom, yields hydroxymethylidyne (COH_{ad}) species. COH_{ad} has the C atom attached to Mo, (CO on-top adsorption), whereas the O is not bonded to the catalyst surface. The adsorption energy for COH_{ad} is -111.62 kcal, making it more stable than CHO_{ad} species on the Mo_6P_3 cluster. COH_{ad} proceeds in the reaction by adding another H atom to C forming hydroxymethylene species. The COH_{ad} route is not energetically favoured ($\Delta E = 50$ kcal/mol) compared to the CHO_{ad} route. If H_{ad} adds to the O atom of COH_{ad}, the C—O bond breaks and H_2O_{ad} and surface adsorbed carbon are produced. Carbon is strongly bound to the surface between two molybdenum atoms and a phosphorus atom. This carbon atom is very difficult to remove from the surface and will eventually deactivate the catalyst (Figure 7).

Based on the above analysis of the reaction intermediates, the PES for CH_4 formation is constructed and depicted in Figure 8, in which the thermochemical data and activation energy of the elementary reaction steps are also shown. Accordingly, the favourable PES pathway for the formation of CH_4 may be summarised as (H_{ad} addition of each step is assumed but not shown): $CO_{ad} \rightarrow CHO_{ad} \rightarrow CH_2O_{ad} \rightarrow CH_2OH_{ad} \rightarrow [CH_{2.ad} + H_2O_{ad}] \rightarrow [CH_{3.ad} + H_2O_{ad}] \rightarrow [CH_4 + H_2O]$.

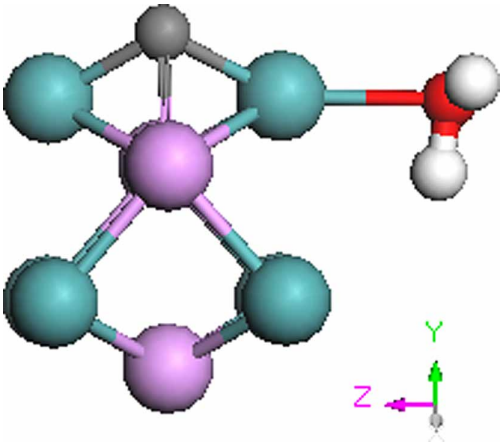

Figure 7. Carbon formation on the Mo_6P_3 cluster.

3.4 *Determining the PES for CH_3OH formation*

Methanol formation occurs via two precursors, CH_2OH_{ad} and CH_2O_{ad}, which are common to CH_4 formation as well. Methanol can be generated from the bridge-bonded CH_2OH_{ad} species by adding H_{ad} to the C atom (Figure 6(XIII)). The Mo—C bond breaks and the C—O bond length is 1.45 Å and the Mo—O bond length is 2.32 Å. The CH_3OH_{ad} adsorption energy is -33.21 kcal, relatively high compared to adsorption energies on other metals as shown in Table 2. CH_3OH_{ad} is attached to a Mo atom through the O atom. The DOS for the CH_3OH–Mo_6P_3 system (Figure 2) shows that the d-orbital (which belongs to Mo) distribution is not altered to a great extent, suggesting that the d-orbital does not have strong overlap with the O atom. Similar behaviour has been observed with other transition metals [38,39]. The main interaction occurs between the p-orbital and the s-orbital. The p-orbital interaction comes mostly from the P atom of the Mo_6P_3 cluster and the oxygen atom. Hence, the adsorption energy of CH_3OH_{ad} on the Mo_6P_3 cluster is higher than other transition metals, i.e. Pt(111), Pd(111), Cu(111), Ni(111), (Table 2) that do not have p-orbitals available. Most of the transition metals show low adsorption energy of CH_3OH due to a small p-orbital contribution to the bond with the O atom. The HOMO energy of CH_3OH–Mo_6P_3 system is -2.48 kcal and the LUMO is -2.25 kcal, whereas, the Fermi energy is 2.25 kcal. The high adsorption energy of CH_3OH_{ad} on the Mo_6P_3 cluster suggests that it may be available for further reaction to form ethanol and other higher carbon-number products. The activation and formation energies for CH_3OH_{ad} via the CH_2OH_{ad} route are 100.91 and 8.45 kcal/mol, respectively.

3.4.1 *Methoxy (CH_3O) and methanol (CH_3OH)*

Addition of H_{ad} to bridge-bonded CH_2O_{ad} yields CH_3O_{ad} species (Figure 6(XIV)), with the carbon atom detached from the metal surface. The C—O bond length is 1.41 Å and the Mo—O bond length is 1.92 Å. The CH_3O_{ad} adsorption energy is -109.08 kcal and the activation energy of this step is 71.13 kcal/mol. Addition of another H_{ad} to the O atom of CH_3O_{ad} yields CH_3OH_{ad} (Figure 6(XV)) with an activation energy of 71.54 kcal/mol and energy of reaction of 36.65 kcal/mol.

The PES pathway for CH_3OH_{ad} formation (Figure 9) follows the route (H_{ad} addition of each step is assumed but not shown) $CO_{ad} \rightarrow CHO_{ad} \rightarrow CH_2O_{ad} \rightarrow CH_2$

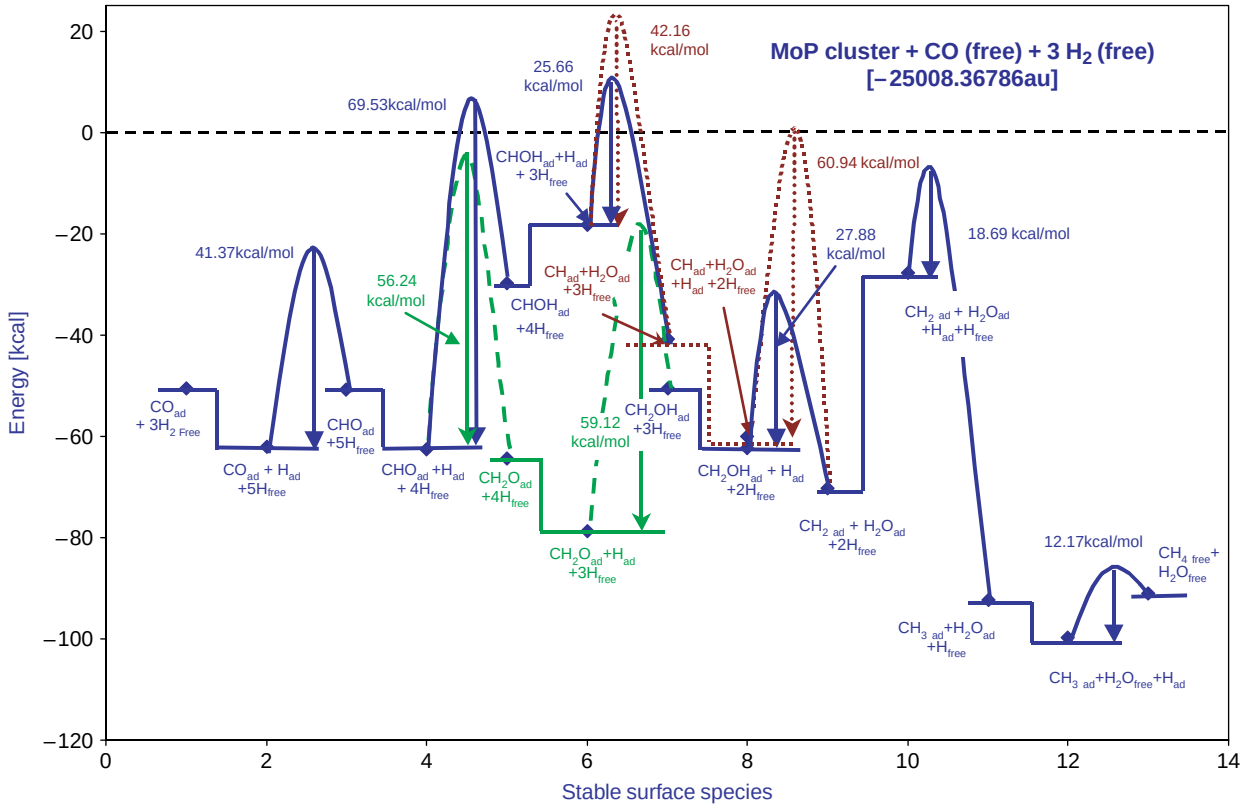

Figure 8. Kinetic pathway of methane formation over Mo_6P_3 cluster.

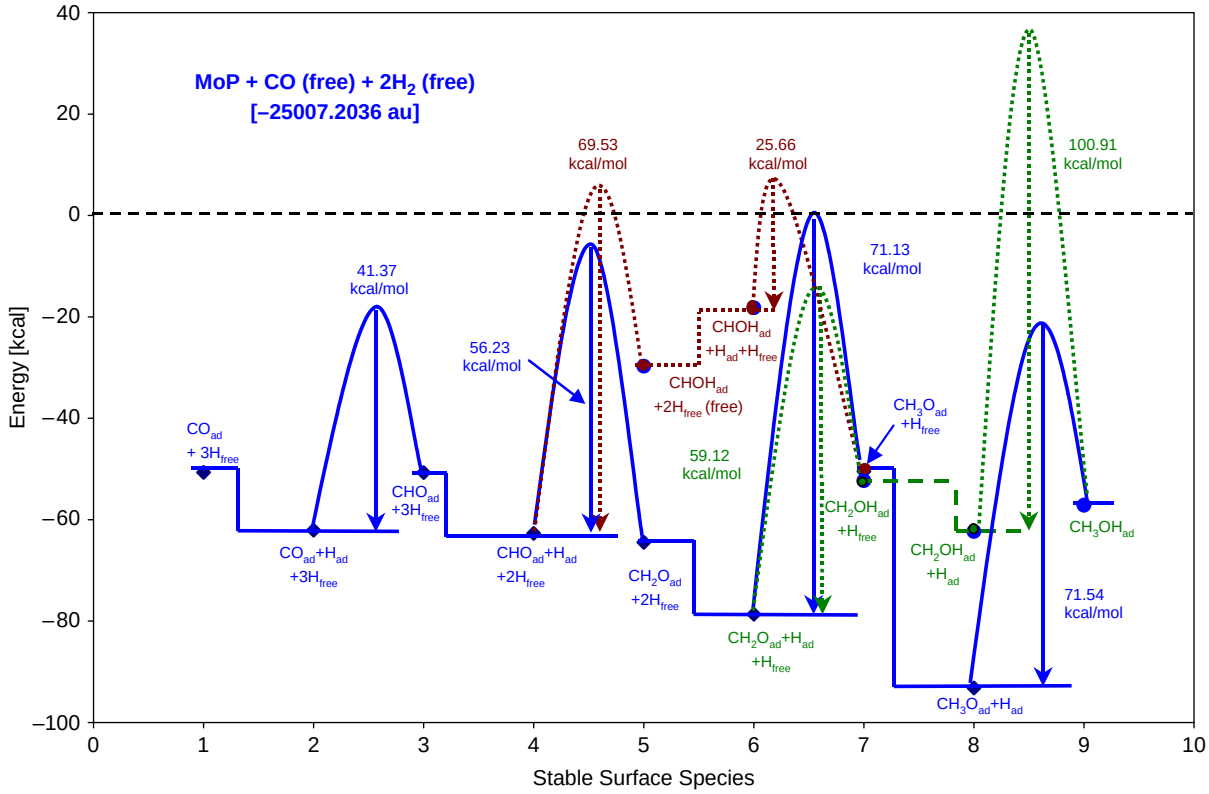

Figure 9. Kinetic pathway of methanol formation over Mo_6P_3 cluster.

$OH_{ad} \rightarrow CH_3OH_{ad}$. This route has the lowest energy surface species up to CH_2OH_{ad}. However, the final step has the largest energy barrier, 100.91 kcal/mol, compared to all other reaction steps. Hence, we conclude that adsorbed CO_{ad} and H_{ad} will form hydroxymethyl but the C—O bond will then break, as the energy barrier is too high to form methanol, resulting in the formation of $CH_{2.ad}$ and water species. This pathway explains the higher selectivity to CH_4 than CH_3OH when synthesis gas is reacted over MoP catalysts [40]. Blocking the CH_4 production path would enhance alcohol production and this may be possible by hindering the approach of a H atom towards the O atom to prevent cleavage of the C—O bond and inhibit water formation. Alkali metals like K should promote this kind of reaction since K provides additional electrons to the nearby O atom and hence, can hinder the formation of H_2O and enhance alcohol production.

Note that the reverse order of the reactions, i.e. the decomposition of methanol and methane over MoP catalysts can also be examined from the data presented herein. Formation of H_2 and CO from CH_3OH follows the decomposition path [$CH_3OH_{ad} \rightarrow CH_3O_{ad} + H_{ad} \rightarrow CH_2O_{ad} + H_{ad} \rightarrow CHO_{ad+}H_{ad} \rightarrow CO_{ad} + H_{ad}$] and from $CH_4 + H_2O$ the path is [$CH_4 + H_2O \rightarrow CH_{3.ad} + H_2O_{ad} \rightarrow CH_{2.ad} + H_2O_{ad} \rightarrow CH_2OH_{ad} \rightarrow CHOH_{ad} \rightarrow COH_{ad} \rightarrow CO_{ad}$]. The same CH_3OH decomposition path is observed on Pt(111) [19] and Ni(111) [36].

3.5 Hydrogen dissociation energy

Both reaction pathways to CH_4 and $CH_3OH_{(ad)}$ formation show that most of the intermediate reaction steps are endothermic. However, both CH_4 and $CH_3OH_{(ad)}$ formation from $CO + H_2$ are exothermic. Heat evolution occurs from adsorption and bond dissociation, whereas bond formation and desorption are endothermic. Bond dissociation can occur between the C—O bond (CH_4 formation), and the H—H bond. The exothermic nature of the reactions is mainly attributed to the dissociation of the hydrogen molecule, which was not included in the energy calculations reported herein. The simulation was accomplished taking a H atom adsorbed on a Mo atom with a stable surface carbon bearing species. The hydrogen molecule adsorbs on 'Mo', and dissociates into atoms that adsorb on two different Mo atoms. The energy released by H—H bond dissociation is -20.56 kcal/mol and the activation energy is 89.34 kcal/mol.

4. Conclusion

A DFT study of CH_4 and CH_3OH formation over an Mo_6P_3 cluster model is described. The Mo_6P_3 cluster was representative of the (100) face of MoP and had similar adsorption energies to MoP. Hydroxymethyl (CH_2OH) is a common intermediate for both CH_4 and CH_3OH formation. However, the energy barrier for CH_3OH formation from CH_2OH was significantly higher than for the formation of methylene and water that leads to CH_4. Thus the simulation predicts the formation of CH_4 rather than CH_3OH over MoP.

Acknowledgements

Financial support from the Natural Sciences and Engineering Research Council (NSERC) of Canada is gratefully acknowledged.

References

[1] A. Gotti and R. Prins, *Basic metal oxides as cocatalysts for Cu/SiO_2 catalysts in the conversion of synthesis gas to methanol*, J. Catal. 178 (1998), pp. 511–519.
[2] E. Iglesia, *Design synthesis, and use of cobalt-based Fischer-Tropsch synthesis catalysis*, Appl. Catal. A: General 161 (1997), pp. 59–78.
[3] R.B. Anderson, *The Fischer–Tropsch Synthesis*, Academic Press, New York, 1984.
[4] J.P. Hindermann, G.J. Hutchings, and A. Kiennemann, *Mechanistic aspects of the formation of hydrocarbons and alcohols from carbon monoxide hydrogenation*, Catal. Rev. Sci. Eng. 35 (1993), pp. 1–127.
[5] P.C. Ellgen, W.J. Bartley, M.M. Bhasin, and T.P. Wilson, *Rhodium-based catalysts for the conversion of synthesis gas to two-carbon chemicals*, Adv. Chem. 178 (1979), pp. 147–157.
[6] S.C. Chuang, J.G. Goodwin, Jr., and I. Wender, *The effect of alkali promotion on CO hydrogenation over Rh/TiO_2*, J. Catal. 95 (1985), pp. 435–446.
[7] A. Kiennemann, R. Breault, J.P. Hindermann, and M. Laurin, *Ethanol promotion by the addition of cerium to rhodium-silica catalysts*, J. Chem. Soc., Faraday Trans. I 83 (1987), pp. 2119–2128.
[8] J. Rieck and A.T. Bell, *Studies of the interactions of H_2 and CO with Pd/SiO_2 promoted with La_2O_3, CeO_2, Pr_6O_{11}, Nd_2O_3, and Sm_2O_3*, J. Catal. 99 (1986), pp. 278–292.
[9] M. Ichikawa, *Catalysis by supported metal crystallites from carbonyl clusters. II. Catalytic ethanol synthesis from carbon monoxide and hydrogen under atmospheric pressure over supported rhodium crystallites prepared from Rh carbonyl clusters deposited on titanium dioxide, zirconium oxide, and lanthanum oxide*, Bull. Chem. Soc. Jpn. 51 (1978), pp. 2273–2277.
[10] B.J. Kip, P.A.T. Smeets, J. van Grondelle, and R. Prins, *Hydrogenation of carbon monoxide over vanadium oxide-promoted rhodium catalysts*, Appl. Catal. 33 (1987), pp. 181–208.
[11] Y. Zhang, Y. Sun, and B. Zhong, *Synthesis of higher alcohols from syngas over ultrafine Mo.Co.K catalysts*, Catal. Lett. 76 (2001), pp. 249–253.
[12] G. Bian, L. Fan, Y. Fu, and K. Fujimoto, *High temperature calcined $K\text{-}MoO_3/\gamma\text{-}Al_2O_3$ Catalysts for mixed alcohol synthesis from syngas: effect of Mo loading*, App. Catal. A 170 (1998), pp. 255–268.
[13] J. Iranmahboob, H. Toghiani, D.O. Hill, and F. Nadim, *The influence of clay on $K_2CO_3/Co.MoS_2$ catalyst in the production of higher alcohol fuel*, Fuel Proc. Tech. 79 (2002), pp. 71–75.
[14] V. Zuzaniuk and R. Prins, *Synthesis and characterization of silica-supported transition-metal phosphides as HDN catalysts*, J. Catal. 219 (2003), pp. 85–96.
[15] A.C. Paul and S.T. Oyama, *Alumina-supported molybdenum phosphide hydroprocessing catalysts*, J. Catal. 218 (2003), pp. 78–87.
[16] S.T. Oyama, *Novel catalysts for advanced hydroprocessing: transition metal phosphides*, J. Catal. 216 (2003), pp. 343–352.
[17] M. Kubo, T. Kubota, C. Jung, M. Ando, S. Sakahara, K. Yajima, K. Seki, R. Belosludov, A. Endou, S. Takami et al., *Design*

of new catalysts for ecological high-quality transportation fuels by combinatorial computational chemistry and tight-binding quantum chemical molecular dynamics approaches, Catal. Today 89 (2004), pp. 479–493.

[18] C.J.H. Jacobsen, S. Dahl, B.S. Clausen, S. Bhan, A. Logadottir, and J.K. Norskov, *Catalyst design by interpolation in the periodic table: bimetallic ammonia synthesis catalysts*, J. Am. Chem. Soc. 123 (2001), pp. 8404–8405.

[19] J. Greeley and M. Mavrikakis, *Competitive paths for methanol decomposition on Pt(111)*, J. Am. Chem. Soc. 126 (2004), pp. 3910–3919.

[20] R. Alcala, M. Mavrikakis, and J.A. Dumesic, *DFT studies for cleavage of C—C and C—O bonds in surface species derived from ethanol on Pt(111)*, J. Catal. 218 (2003), pp. 178–190.

[21] A.A. Gokhale, S. Kandoi, J.P. Greeley, M. Mavrikakis, and J.A. Dumesic, *Molecular-level descriptions of surface chemistry in kinetic models using density functional theory*, Chem. Eng. Sci. 59 (2004), pp. 4679–4691.

[22] S. Kandoi, J. Greeley, A.M. Sanchez-Castillo, S.T. Evans, A.A. Gokhale, J.A. Dumesic, and M. Mavrikakis, *Prediction of experimental methanol decomposition rates on platinum from first principles*, Top. Catal. 37 (2006), pp. 17–28.

[23] B. Delley, *From molecules to solids with the $DMol_3$ approach*, J. Chem. Phys. 113 (2000), pp. 7756–7764.

[24] A.D. Becke, *A multicenter numerical integration scheme for polyatomic molecules*, J. Chem. Phys. 88 (1988), pp. 2547–2553.

[25] J.P. Perdew and Y. Wang, *Accurate and simple analytic representation of the electron-gas correlation energy*, Phys. Rev. B 45 (1992), pp. 13244–13249.

[26] W. Kohn and L.J. Sham, *Self-consistent equations including exchange and correlation effects*, Phys. Rev. A 140 (1965), pp. 1133–1138.

[27] P. Pulay, *Improved SCF convergence acceleration*, J. Comp. Chem. 3 (1982), pp. 556–560.

[28] B. Delley, in *Modern Density Functional Theory: A Tool for Chemistry, Theoretical and Computational Chemistry*, Vol. 2, J.M. Seminorio and P. Politzer, eds., Elsevier Science, Amsterdam, 1995.

[29] S. Bell and J.S. Crighton, *Locating transition states*, J. Chem. Phys. 80 (1984), pp. 2464–2475.

[30] S. Fischer and M. Karplus, *Conjugate peak refinement: an algorithm for finding reaction paths and accurate transition states in systems with many degrees of freedom*, Chem. Phys. Lett. 194 (1992), pp. 252–261.

[31] G. Henkelman and H. Jonsson, *Improved tangent estimate in the nudged elastic band method for finding minimum energy paths and saddle points*, J. Chem. Phys. 113 (2000), pp. 9978–9985.

[32] Z. Feng, C. Liang, W. Wu, Z. Wu, A.R. Santen, and C. Li, *Carbon monoxide adsorption on molybdenum phosphides: Fourier transform infrared spectroscopic and density functional theory studies*, J. Phys. Chem. B 107 (2003), pp. 13698–13702.

[33] P. Liu and J.A. Rodriguez, *Catalytic properties of molybdenum carbide, nitride and phosphide: a theoretical study*, Catal. Lett. 91 (2003), pp. 247–252.

[34] M. Neurock, *First-principles analysis of the hydrogenation of carbon monoxide over palladium*, Top. Catal. 9 (1999), pp. 135–152.

[35] J.G. Nunan, C.E. Bogdan, K. Klier, K.J. Smith, C. Young, and R.G. Herman, *Higher alcohol and oxygenate synthesis over cesium-doped Cu/ZnO catalysts*, J. Catal. 116 (1989), pp. 195–221.

[36] I.N. Remediakis, F. Abild-Pedersen, and J.K. Norskov, *DFT study of formaldehyde and methanol synthesis from CO and H_2 on Ni(111)*, J. Phys. Chem. B 108 (2004), pp. 14535–14540.

[37] J. Greeley, A.A. Gokhale, J. Kreuser, J.A. Dumesic, H. Topsoe, N.Y. Topsoe, and M. Mavrikakis, *CO vibrational frequencies on methanol synthesis catalysts: a DFT Study*, J. Catal. 213 (2003), pp. 63–72.

[38] R. Hoffmann, *A chemical and theoretical way to look at bonding on surfaces*, Rev. Mod. Phys. 60 (1988), pp. 601–628.

[39] D. Zeroka and R. Hoffmann, *Adsorption of methoxy on Cu(100)*, Langmuir 2 (1986), pp. 553–558.

[40] S.F. Zaman and K.J. Smith, *Synthesis gas conversion to alcohols on MoP catalysts*, Book of abstracts, 19th Canadian Symposium on Catalysis, 2006, p. 32.